한국소음진동공학회논문집 제 17 권 제 12 호, pp. 1152~1160, 2007.

A Design of Integral Sliding Mode Suspension Controller to Reject the Disturbance Force Acting on the Suspension System in the Magnetically Levitated Train System

자기부상 열차 시스템에서 추진 장치에서 발생하는 부상 간섭력의 영향을 제거하기 위한 적분형 Sliding Mode 부상 제어기 설계

Jun-Ho Lee†
이 준 호

(Received September 4, 2007 ; Accepted December 7, 2007)

Key Words : Magnetically Levitated System(자기부상시스템), Control System(제어시스템), Sliding Mode Controller(슬라이딩모드제어기), Linear Induction Motor(선형유도모터)

ABSTRACT

In this paper we deal with a design of integral sliding mode controller to reject the disturbance force acting on the suspension system in the magnetically levitated system which is propelled by the linear induction motor. The control scheme comprises an integral controller which is designed for achieving zero steady-state error under step disturbances, and a sliding mode controller which is designed for enhancing robustness under plant uncertainties. A proper continuous design signal is introduced to overcome the chattering problem. The disturbance force produced by the linear motor is formularized by using a curve fitting of the experimental raw data. Computer simulations show the effectiveness of the designed integral sliding mode controller to reject the disturbance force.

요 약

이 논문에서는 선형 유도 모터로 추진되는 자기부상 열차 시스템에서 열차의 속도에 따라서 추진 시스템으로부터 발생하는 간섭력의 부상 시스템에 대한 영향을 최소화하기 위한 적분형 sliding mode 부상제어기의 설계에 대해서 다룬다. 제어기 구조는 적분형 제어기와 sliding mode 제어기로 구성된다. 적분형 제어기는 정적 외란에 대해서 정상상태 오차가 영에 도달하는 것을 보장하고 sliding mode 제어기는 수학적 모델이 본질적으로 갖고 있는 불확실성에 대한 강건성을 보장 한다 또한 sliding mode 제어기의 chattering 문제를 해결하기 위해서 연속 함수를 도입한다. 선형 유도모터에 의한 간섭력은 실험 데이터의 curve fitting에 의한 수학적 모델링을 통하여 수식화 한다. 컴퓨터 모의시험을 통해서 설계된 적분형 sliding mode 제어기의 효용성을 보인다.

1. Introduction

One of the ways that non-contact states between two materials are maintained is to employ a magnetic suspension technology[1].

† Corresponding Author: Member, Korea Railroad Research Institute
E-mail : jhlee77@krri.re.kr
Tel : 82-31-460-5040, Fax : 82-31-460-5449

This system is commonly known as Magnetically Levitated system (Maglev) which has been used in the vehicle levitation system and magnetic bearing system developed in the University of Virginia, U.S.A. in 1937 for the first time. There are various applications employing the magnetic levitation configuration as a key technology, such as the magnetically levitated train system[1,7], the high speed turbo compressors[2,5], the flywheel energy storage system[3,4], and the artificial heart pump[6].

The magnetically levitated train system can be divided into two parts based on the levitation method: one is a repulsive type using super conductors. One of the disadvantages of this type of suspension system is that it is needed for operation below the critical speed when the suspended object is stationary. The other type is electromagnetic suspension system (EMS system) using ferromagnetic or permanent magnet. The type has one significant advantage in that it provides attraction force at zero speed, but such system is inherently unstable. In order to overcome the inherent instability an active controller plays a very important role in the electromagnet suspension system to make the stable suspension and to maintain the suspended object within the nominal air gap[1].

Especially, the external disturbance force acting on the controller in the magnetically levitated train system may cause the malfunction of the suspension system[8]. If a Maglev train is propelled by the linear induction motor, the suspension controller of the Maglev train should have a capability to reject the normal force produced from the linear induction motor. The reason is because the normal force of the linear induction motor acts as the disturbance force on the suspension controller.

In this paper, we deal with a design procedure for the integral sliding mode controller to reject the disturbance force acting on the suspension controller[4~6]. First, we present a simple mathematical model for the Maglev train and then introduce the integral sliding mode controller. Second, a mathematical formula for the normal force of the linear induction motor is derived by the curve fitting of the experimental data. Finally, we show the effectiveness of the integral sliding mode controller to reject the disturbance force by the simulations.

2. Fundamental Mathematical Model

Figure 1 shows a simple schematic diagram for EMS system which has the electromagnets

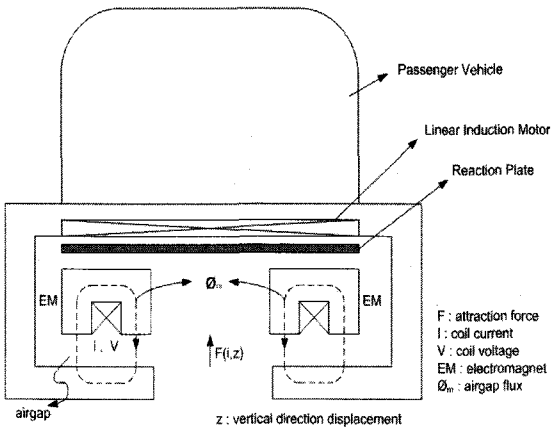

Fig. 1 Schematic diagram for EMS system

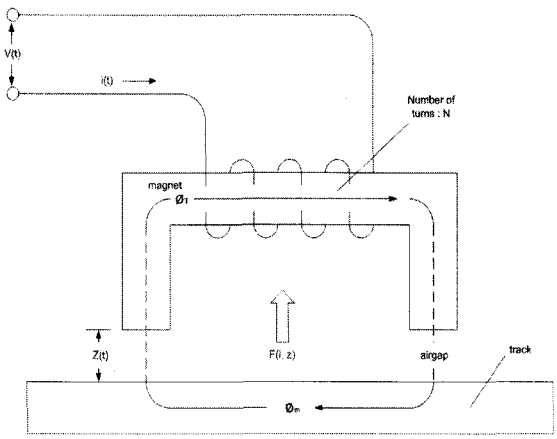

Fig. 2 Simplified schematic diagram

as the suspension actuators, linear induction motor and reaction plate for the vehicle propulsion. As shown in Fig. 1, the passenger vehicle and the bogie can be levitated by the electromagnets attraction force. Once the bogie is levitated, the propulsion system with linear induction motor and reaction plate is activated to move the passenger vehicle.

Figure 2 is the simplified equivalent model of the suspension system shown in Fig. 1.

The mathematical model of this system is divided into two parts: One is the plant (mechanical) dynamics and the other is the actuator dynamics.

The plant dynamics is

$$m\ddot{z} = F(i,z) - mg - f_d \tag{1}$$

where m is the total mass of the controlled object, g is the gravitational acceleration, and f_d is the external disturbance force acting on the controlled object. In Eq. (1), $F(i,z)$ is the electromagnets attraction force which is proportional to the current deviation and inversely proportional to the air gap deviation, expressed such as:

$$F(i,z) = \frac{B^2 A}{\mu_0} = \frac{\mu_0 N^2 A}{4}\left(\frac{i(t)}{z(t)}\right)^2 \tag{2}$$

where B is the flux density of the magnetic core material, A is the cross sectional area of the pole face of the electromagnet, μ_0 is the permeability in the air space, and N is the number of turns.

Since Eq. (2) has high nonlinearity it is necessary that the linear approximation should be carried out for the analysis of Eq. (2) with respect to the nominal point (i_0, z_0). The Taylor Series Expansion is usually employed and the Eq. (2) becomes

$$F(i,z) = k_i i(t) + k_z z(t) \tag{3}$$

where $k_i = \frac{\mu_0 N^2 A i_0}{2z_0^2}$ and $k_z = -\frac{\mu_0 N^2 A i_0^2}{2z_0^3}$.

The actuator dynamics is

$$\begin{aligned} v(t) &= Ri(t) + \frac{d}{dt}[L(i,z)i(t)] \\ &= Ri(t) + \frac{\mu_0 N^2 A}{2z_{0(t)}}\frac{d}{dt}i(t) - \frac{\mu_0 N^2 A i_0}{2z_{0(t)}^2}\frac{d}{dt}z(t) \end{aligned} \tag{4}$$

where v is the coil voltage, R is the coil resistance, and $L(i,z)$ is the magnet inductance which is the function of the air gap displacement such as $L(i,z) = \frac{\mu_0 N^2 A}{2z_{0(t)}}$. There is a variation of the inductance with respect to the air gap displacement in the second term , and that the third term denotes a voltage which varies with changes in the air gap $z(t)$ and its rate of change similar to back EMF voltage.

By using Eqs. (1), (3), and (4) the state space equations are written in vector matrix form:

$$\begin{bmatrix} \dot{z} \\ \ddot{z} \\ \dot{i} \end{bmatrix} = \begin{bmatrix} 0 & 1 & 0 \\ \frac{-k_z}{m} & 0 & \frac{k_i}{m} \\ 0 & \frac{k_z}{k_i} & \frac{-R}{L} \end{bmatrix} \begin{bmatrix} z \\ \dot{z} \\ i \end{bmatrix} + \begin{bmatrix} 0 \\ 0 \\ \frac{1}{L} \end{bmatrix} v + \begin{bmatrix} 0 \\ \frac{1}{m} \\ 0 \end{bmatrix} f_d \tag{5}$$

where f_d is the normal force of the linear induction motor. In this paper we ignore the static gravitational force. Eq. (5) can be simply expressed as

$$\dot{x}(t) = Ax(t) + Bu(t) + Ef_d(t) \tag{6}$$

where

$$A = \begin{bmatrix} 0 & 1 & 0 \\ \frac{-k_z}{m} & 0 & \frac{k_i}{m} \\ 0 & \frac{k_z}{k_i} & \frac{-R}{L} \end{bmatrix},\ B = \begin{bmatrix} 0 \\ 0 \\ \frac{1}{L} \end{bmatrix},\ E = \begin{bmatrix} 0 \\ \frac{1}{m} \\ 0 \end{bmatrix}$$

3. Integral Sliding Mode Controller

To enhance the disturbance rejection ability of the control system, we introduce an integrator as a state variable into (5). The integrator output z_i is expressed as the difference between the integrated reference position r and integrated position z written as:

$$z_i = \int (r - z) dt \tag{7}$$

where r is zero for a nominal design. The block diagram of the proposed control system is shown in Fig. 3.

In order to synthesize the integral sliding mode controller we write the state variables as $x = [z_i \quad z \quad \dot{z} \quad i]$, and get the following state space matrices.

$$A = \begin{bmatrix} 0 & -1 & 0 & 0 \\ 0 & 0 & 1 & 0 \\ 0 & \frac{-k_z}{m} & 0 & \frac{k_i}{m} \\ 0 & 0 & \frac{k_z}{k_i} & \frac{-R}{L} \end{bmatrix}, \quad B = \begin{bmatrix} 0 \\ 0 \\ 0 \\ \frac{1}{L} \end{bmatrix}, \quad E = \begin{bmatrix} 0 \\ 0 \\ \frac{1}{m} \\ 0 \end{bmatrix} \tag{8}$$

Equation (8) is decomposed as:

$$\begin{bmatrix} \dot{x}_1 \\ \dot{x}_2 \end{bmatrix} = \begin{bmatrix} A_{11} & A_{12} \\ A_{21} & A_{22} \end{bmatrix} \begin{bmatrix} x_1 \\ x_2 \end{bmatrix} + \begin{bmatrix} B_1 \\ B_2 \end{bmatrix} u \tag{9}$$

where

$$x_1 = \begin{bmatrix} z_i \\ z \\ \dot{z} \end{bmatrix}, \quad x_2 = i$$

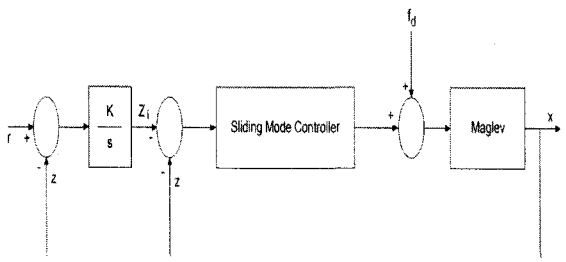

Fig. 3 Block diagram of an integral sliding mode controller for Maglev

$$A_{11} = \begin{bmatrix} 0 & -1 & 0 \\ 0 & 0 & 1 \\ 0 & \frac{-k_z}{m} & 0 \end{bmatrix}, \quad A_{12} = \begin{bmatrix} 0 \\ 0 \\ \frac{k_i}{m} \end{bmatrix}$$

$$A_{21} = \begin{bmatrix} 0 & 0 & \frac{k_z}{k_i} \end{bmatrix}, \quad A_{22} = -\frac{R}{L} \tag{10}$$

$$B_1 = \begin{bmatrix} 0 \\ 0 \\ 0 \end{bmatrix}, \quad B_2 = \frac{1}{L}, \quad u = v$$

Let the switching surface be defined as $\sigma = Sx$ where

$$\sigma = [S_1 \quad S_2] \begin{bmatrix} x_1 \\ x_2 \end{bmatrix}, \quad S_1 \in R^{1\times 3}, \quad S_2 = R \tag{11}$$

If the system dynamics is an ideal sliding surface we have $\sigma = Sx = 0$. Using this property we can determine the equivalent system and linear control input. $\sigma = 0$ yields

$$x_2 = -\frac{S_1}{S_2} x_1 \tag{12}$$

Substituting (12) into (9) yields the equivalent system

$$\dot{x}_1 = (A_{11} - A_{12} S_2^{-1} S_1) x_1 \tag{13}$$

Defining $k = S_2^{-1} S_1$, we write (13) as

$$\dot{x}_1 = (A_{11} - A_{12} k) x_1 \tag{14}$$

The location of poles of the resulting system are obtained by selecting k and S_2 as the switching function becomes $\sigma = Sx$, $S = [S_1 \quad S_2] = [S_2 k \quad S_2] = S_2 [k \quad 1]$. Since (A_{11}, A_{12}) is controllable, a pole placement method is employed to select the gain k in (14). The sliding mode control inputs are separated into the linear and nonlinear components as $u = u_l + u_{nl}$. The linear input u_l can be selected by the following equations:

$$\dot{x} = Ax + Bu \tag{15}$$

$$\dot{\sigma} = S\dot{x} = 0 \tag{16}$$

From Eqs. (15) and (16) the equivalent linear control input is

$$u_l = -(SB)^{-1}SAx = -F_l x \tag{17}$$

The sliding mode reaching condition given by $\sigma\dot{\sigma} < 0$ brings the system dynamics to the sliding surface $\sigma = 0$. Choose the nonlinear control as $u_{nl} = -(SB)^{-1}\rho sgn(\sigma)$ where $\rho > 0$. Then, it follows that

$$\begin{aligned}\sigma\dot{\sigma} &= \sigma S(Ax + Bu)\\ &= \sigma SAx - \sigma SB[(SB)^{-1}SAx + (SB)^{-1}\rho sign(\sigma)]\\ &= -\rho\sigma sgn(\sigma)\end{aligned} \tag{18}$$

The control input can then be written as

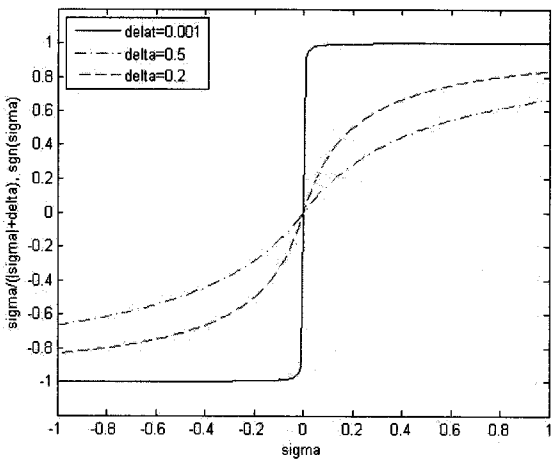

Fig. 4 Smooth approximation of the sgn function

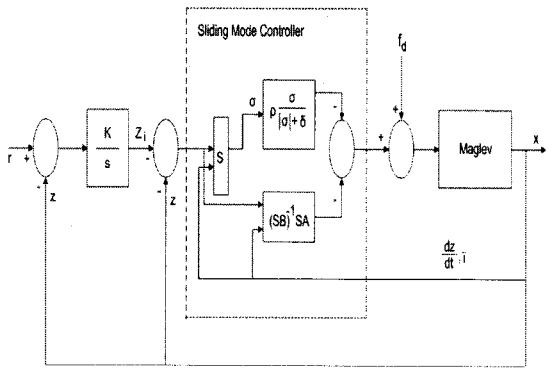

Fig. 5 Block diagram of integral sliding mode control implementation

$$u = -(SB)^{-1}[SAx + \rho sgn(\sigma)] \tag{19}$$

In practice, a discontinuous control component as $sgn(\sigma)$ is undesirable because it may cause a chattering problem. A common choice of a practical nonlinear control input is

$$U_{nl} = -\rho\frac{\sigma}{|\sigma| + \delta} \tag{20}$$

where δ is the boundary layer which is selected to reduce the chattering problem and ρ is a design parameter.

Figure 4 shows the relation between the discontinuous sgn function and continuous function. It is represented that the slope of the continuous function depends upon δ. Figure 5 shows the block diagram of the designed sliding mode controller connected to the integral compensator.

4. Curve Fitting for the Normal Force

The linear induction motor is composed of primary coil and reaction plate as secondary. The thrust force and the normal force are dependant upon the relative displacement of primary and the secondary[7]. The relative motion between the rotor and the stator can be expressed by introducing slip as follows.

$$s = \frac{n_{slip}}{n_{sync}} \times 100\% \tag{21}$$

and

$$s = \frac{n_{sync} - n_m}{n_{sync}} \times 100\% \tag{22}$$

where s is the slip, n_{slip} is the slip speed of the motor, n_{sync} is the synchronized rotor speed, and n_m is the mechanical rotor speed. If the end effect is ignored the force property of the linear induction motor is dependant on the

slip frequency which is defined as the difference in speed between the synchronized rotor speed and the mechanical rotor speed as:

$$n_{silp} = n_{sync} - n_m \tag{23}$$

(22) and (23) yield

$$n_m = (1-s)n_{sync} \tag{24}$$

Equation (24) shows that $n_m = n_{sync}$ and $s = 0$ are satisfied if the mechanical speed of the rotor is equal to the synchronized rotor speed, on the other hand $n_m = 0$ and $s = 1$ are satisfied if the mechanical rotor speed is zero.

Figure 6 shows the relation between force and slip. As shown in the figure the mechanical speed goes down as the slip increases. Fig. 7 shows the relation between the mechanical speed and the force produced by the linear induction motor. When the mechanical rotor speed is low as slip is close to one, the flux density is increased and the normal force acts as the attractive force in the linear motor, which acts as the external disturbance force against the suspension system. On the other hand, when the mechanical rotor speed goes up the flux density is decreased and the normal force acts as the repulsive force in the linear motor which causes decrease of the suspension control current. Therefore, the normal force is dependant upon the mechanical rotor speed and it is necessary to reduce the attractive force acting on the suspension system as the external disturbance force by the slip frequency control.

For the simulation of the Fig. 7, we got the force data from the report[7].

Figure 8 shows the estimated normal force by using the curve fitting method. Equation (25) represents the approximated formula which expresses the normal force.

$$F_n = p_1 v_m^2 + p_2 v_m + p_3 \tag{25}$$

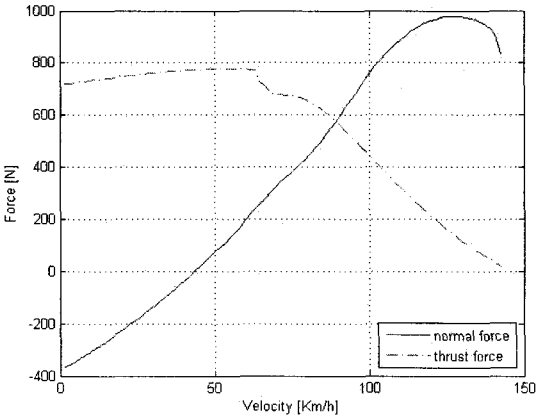

Fig. 7 Relation between the mechanical velocity and force

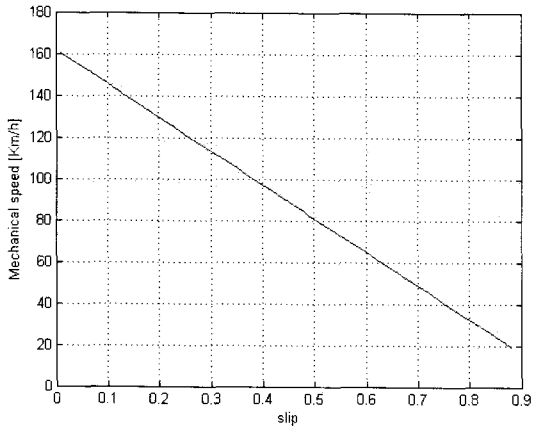

Fig. 6 Slip and mechanical speed

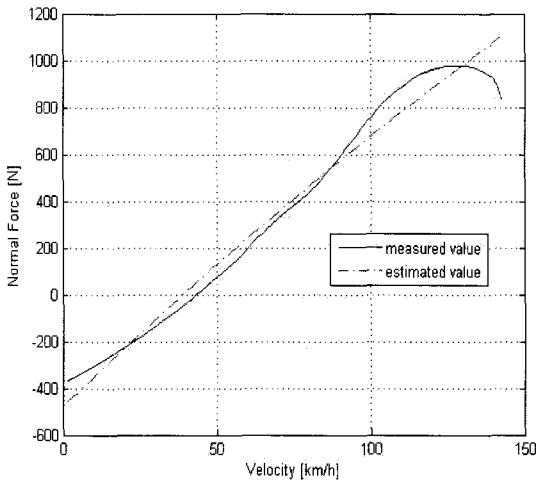

Fig. 8 Estimated force

where F_n is the normal force, p_i, $i=1,2,3$, is the coefficient for the approximation, and v_m is the mechanical velocity. Equation (25) and Fig. 8 show the attractive force is maximum when v_m is zero. Since the flux density in the air gap of the linear induction motor is increased in the low speed range the attractive normal force is increased. This means that the direction of the force between the normal force and the levitation force is opposite (see Fig. 1). However the direction between two forces are the same in the high speed range because of the decrease of the flux density in the air gap. This analysis represents that the suspension controller is affected by the 500 N attractive normal force of the linear motor which acts as the external disturbance force at low speed.

5. Simulations

Table 1 shows the parameters for the EMS type suspension system. The attractive force which acts on the suspension system as the external disturbance force is produced at low speed range, that is from 0 km/h to 40 km/h. The integral sliding mode controller should be designed to reject the external disturbance force. The highest value of the attractive force is produced from 0 km/h to 10 km/h as shown in Fig. 8. Therefore in the simulations external disturbance force of 1,000 N or 1,500 N are input to the suspension system at 1 sec. Figure 9 and Fig. 10 show the simulation results. Even if 1,000 N and 1,500 N are input to the suspension system at 1 sec, the integral sliding mode controller suppresses well the external disturbance force. For the integral sliding mode controller the following values are set for Eqs. (14) and (20) as:

$$k=10^5\times[0.0161 \quad 0.006 \quad 1.357]$$
$$\rho=50, \quad \delta=0.4$$

Figure 11 and Fig. 12 represent the input voltage for the 1,000 N and 1,500 N of the

Table 1 Parameters for suspension system

Parameters	Values
Turns[N]	280
Coil resistance[Ω]	0.16
Steady current[A]	35
Pole face area[m^2]	4273×10^{-6}
Nominal gap[m]	10×10^{-3}
Coil inductance[H]	0.02
Vehicle mass[kg]	500

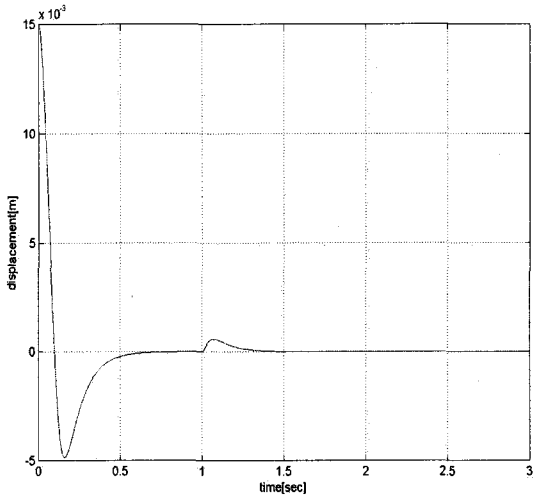

Fig. 9 External disturbance force rejection(1,000 N)

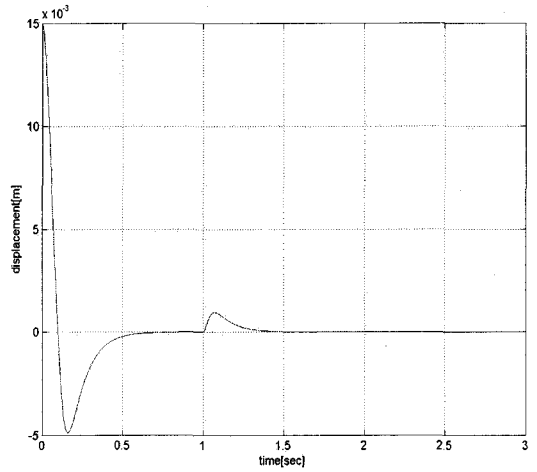

Fig. 10 External disturbance force rejection(1,500 N)

external disturbance force. In the initial states of the both figures the chattering is shown due to the controller gains that are tuned for the rejection of the external disturbance acting on the suspension system at time 1 sec. Even if the external disturbance effect on the system at time 1 sec it presents that the control input voltage is stable.

Figure 13 and Fig. 14 show the dynamic simulations that the disturbance force acts on the integral sliding mode controller dynamically. The dynamic simulation model makes it possible that the effect of the normal force of the linear induction motor on the controller can be observed in the overall mechanical rotor speed range. Figure 13 represents the gap deviation when the integral sliding mode controller is employed. To apply the disturbance force to the suspension system Eq. (25) is used in the change of the mechanical speed v_m from 0 km/h to 160 km/h with a constant traction force. Since Eq. (25) provides the normal force as a function of the mechanical speed, it is possible to observe the effect of the normal force on the controller in the overall speed range. As shown in Fig. 13 Maglev vehicle is successfully suspended from the initial position (15×10^{-3} m) even if the normal force of the linear induction motor acts on the suspension system as the external disturbance force, and the gap

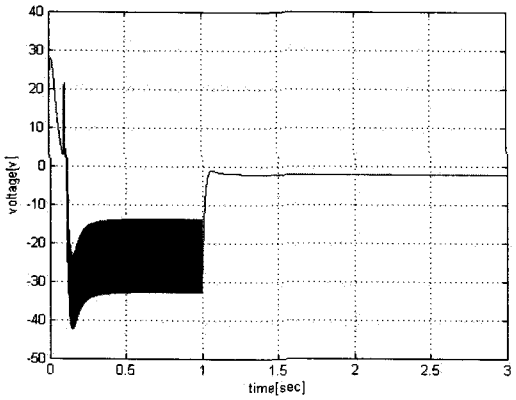

Fig. 11 Input voltage for 1,000 N external disturbance

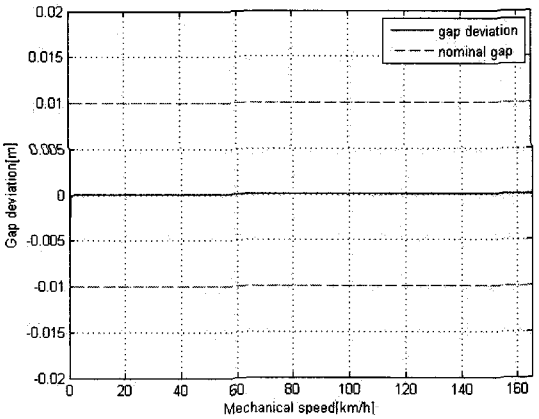

Fig. 13 Gap deviation by dynamic simulation

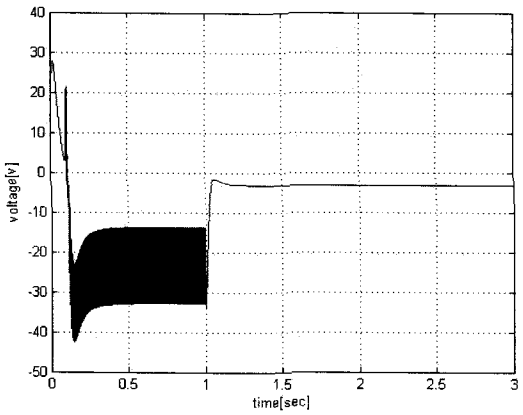

Fig. 12 Input voltage for 1,500 N external disturbance

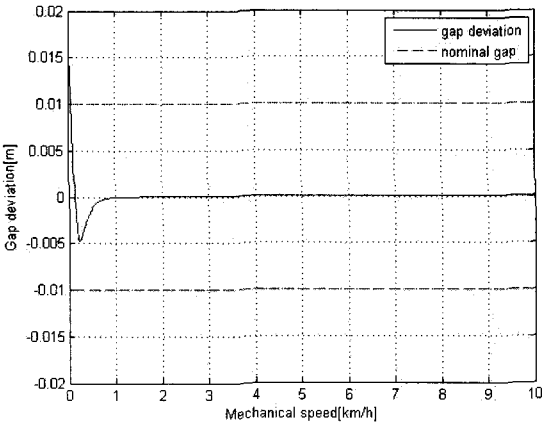

Fig. 14 Gap deviation(rescaled) by dynamic simulation

deviation is maintained inside the nominal gap. Fig. 14 shows the rescaled of Fig. 13 to observe the low speed range.

6. Conclusions

In this paper, we dealt with the external disturbance force rejection property of the sliding mode controller in the magnetically levitated train system with the linear induction motor for propulsion system. The external disturbance force is produced from the linear induction motor at low speed.

The fundamental mathematical model of the magnetically levitated train was shown and then the force analysis of the linear induction motor with the curve fitting method was presented.

The effective method of the integral sliding mode controller to suppress the external disturbance force was suggested and shown by the simulations.

It is possible for the integral sliding mode controller proposed in this paper to be applied for the system employing magnetic levitation technology such as the artificial heart pump[6], the energy storage high speed fly wheel system, and high speed turbo compressor.

References

(1) The Magnetically Levitation Technical Committee of The Institute of Electrical Engineers of Japan, 1993, "Magnetic Suspension Technology: Magnetic Levitation System and Magnetic Bearings", CORONA PUBLISHING CO.

(2) Nonami, K., Fan, Q., Ueyama, H., 1998, "Unbalance Vibration Control of Magnetic Bearing Systems Using Adaptive Algorithm with Disturbance Frequency Estimation", 6th ISMB.

(3) Lee, J.-H., Kang, M.-S., Chung, Y.-W., Lee, J.-S., Lee, K.-S., 2000, "Displacement Sensorless Control of Magnetic Bearing System Using Current and Magnetic Flux Feedback", The Transactions of the Korea Institute of Electrical Engineers D, Vol. 49D, No. 7, pp. 339~345.

(4) Lee, J.-H., Allaire, P. E., Tao, G., Zhang, X., 2003, "Integral Sliding Mode Control of a Magnetically Suspended Balance Beam: Analysis , Simulation and Experimentation", IEEE Trans. On Mechatronics, Vol. 6, No. 3, pp. 338~346.

(5) Fang, Y., Feemster, M., Dawson, D., 2003, "Nonlinear Disturbance Rejection for Magnetic Levitation Systems", Proceedings of the 2003 IEEE International Symposium on Intelligent Control, Huston, Texas.

(6) Lee, J.-H., Allaire, P. E., Tao, G., Decker, J. A., Zhang, X., 2003, "Experimental Study of Sliding Mode Control for a Benchmark Magnetic Bearing System and Artificial Heart Pump Suspension", IEEE Transactions on Control System Technology, Vol. 11, No. 1, pp. 128~138.

(7) Jeong, H.-G., 1995, "Development of Maglev System for Urban Transit Application", Korea Institute of Machinery & Materials Final Report.

(8) Lee, J.-H., Kim, J.-K., Lee, K.-S., 2006, "A Study on the Rejection of Dynamic Disturbance Force in a Magnetically Suspended System Using Flux Feedback", Transactions of the Korean Society of Noise and Vibration Engineering, Vol, 16, No, 3 pp. 283~290.